applied optics

Modeling and implementation of a fiber-based quartz-enhanced photoacoustic spectroscopy system

Yongjiang Dong,[1,2,†] Jian Chen,[1,2,†] Longqiang Luo,[1,2] Erik Forsberg,[1,2] Sailing He,[1,2] and Chunsheng Yan[1,2,*]

[1]State Key Laboratory for Modern Optical Instrumentation, Centre for Optical and Electromagnetic Research, Zhejiang University, Zhejiang, China
[2]Provincial Key Laboratory for Sensing Technologies, JORCEP [Joint Research Center of Photonics of the Royal Institute of Technology, Lund University and Zhejiang University], Zhejiang University, Hangzhou 310058, China
*Corresponding author: yancs@zju.edu.cn

Received 28 January 2015; revised 1 April 2015; accepted 6 April 2015; posted 9 April 2015 (Doc. ID 233394); published 29 April 2015

A compact fiber-based quartz-enhanced photoacoustic spectroscopy system requiring no extra optical lens has been developed for the detection of acetylene. The system is based on a common fiber or an axicon fiber to conduct the light. Experimental results show comparable detection sensitivity to that of tapered fiber-based photoacoustic spectroscopy systems. The system is easy to adjust and has low insertion loss and is thus well suited for small portable sensor applications in the future. A numerical model based on actual beam profiles was furthermore developed as part of the study to investigate the optimal positions of the fibers and to verify the experimental results. © 2015 Optical Society of America

OCIS codes: (060.2370) Fiber optics sensors; (300.1030) Absorption; (120.4820) Optical systems.

http://dx.doi.org/10.1364/AO.54.004202

1. INTRODUCTION

Photoacoustic spectroscopy (PAS) uses an acoustic transducer to detect ultrasonic signals produced by light absorptions of gas molecules under investigation and is an effective method for trace gas detection with high sensitivity and selectivity [1–3]. Compared with traditional PAS, which usually uses a microphone with a large resonant acoustic cell [4,5], quartz-enhanced photoacoustic spectroscopy (QEPAS), first reported by Kosterev *et al.* [6], has been proved to be a more compact and robust technique with comparable sensitivity [7–9]. In a QEPAS system, a quartz tuning fork (QTF) with small size, low cost, and extremely high Q factor is used as an acoustic transducer [10]. A QTF is immune to ambient noise due to its high resonant frequency, and is because of this able to detect very small gas samples (few cubic millimeters in volume). Thus QEPAS has been widely used for all kinds of trace gas detection with on-beam or off-beam configurations in recent years [11–16].

However, the QEPAS systems reported to date are almost all based on open free-space path configurations, which require complex and precise optical collimation and focus systems to obtain high photoaoustic generation efficiency. Recently, a compact evanescent-wave PAS (EPAS) gas detection system based on a tapered optical fiber (TOF) was developed, which showed lower insertion loss while at the same time being easier to align [17]. In EPAS, photoacoustic pressure is excited by the evanescent wave of the micro/nano fiber. However, the TOFs need to be fabricated through a complex flame-brushing technique [18], and fiber tapers with subwavelength diameters are also quite fragile. In this work, a QEPAS system based on common single-mode fibers, which has the same advantages as and comparable sensitivity to EPAS systems while being more stable and flexible, has been developed. The same system was also studied having replaced the common fiber with an axicon fiber [19] to investigate whether this could increase the systems' photoacoustic excitation efficiency while retaining its easily adjustable configuration.

For the purpose of system optimization and validation of experimental results our work also includes the extension of previous numerical studies of QEPAS systems. Petra *et al.* [20] developed an analytical model of the QTF by which the optimal position of the laser source to induce the strongest photoacoustic signal was investigated. Numerical simulations of a similar structure using the COMSOL Multiphysics software were performed by Cao *et al.* [21]. Related studies on modeling of QEPAS have been performed by Firebaugh *et al.* [22], Petra *et al.* [23], and Yi *et al.* [24]. However, an approximation was made, or a simplistic model used, of the laser beam profiles in all previous studies. By contrast, in this paper, a numerical model that considers the actual emergent light beam

profile from the fibers is developed and used. Using this model the optimal three-dimensional fiber location relative to the QTF has been studied and compared to the corresponding experiment results.

2. THEORY AND NUMERICAL MODELING

The pressure p of the acoustic wave generated by the interaction between trace gas and laser beams satisfies the acoustic wave equation

$$\frac{\partial^2 p}{\partial t^2} - c^2 \nabla^2 p = S, \tag{1}$$

where t is the time, and c is the speed of sound. S is the acoustic intensity, which relates to the laser intensity I according to

$$S = \alpha(\gamma - 1)\frac{\partial I}{\partial t}, \tag{2}$$

where α is the absorption coefficient and γ is the adiabatic coefficient. Thus, in frequency space, the distribution of the acoustic source power is proportional to that of the laser power.

For a common single-mode fiber with a flat end the output optical intensity distribution I can be expressed as [25]

$$I(\rho, l) = \frac{2P}{\pi W_0^2\left(1 + \left(\frac{\lambda l}{\pi W_0^2}\right)^2\right)} \exp\left[-\frac{2\rho^2}{W_0^2\left(1 + \left(\frac{\lambda l}{\pi W_0^2}\right)^2\right)}\right], \tag{3}$$

where ρ and l are the cylindrical coordinates of the output light. P and λ represent the total power and wavelength of the laser, respectively, while W_0 denotes the Gaussian beam waist. The emergent beam from axicon fiber with a focusing effect can be expressed as [26]

$$I(\rho, l) = \frac{4Pkl \sin^2 \alpha_0}{W_0^2 \cos \alpha_0} J_0^2(k\rho \sin \alpha_0) \exp\left(-\frac{2l^2 \tan^2 \alpha_0}{W_0^2}\right), \tag{4}$$

where k is angular wavenumber and α_0 is the polar angle of the axicon.

The numerical simulation is based on the finite element method, which utilizes the Acoustic-Structure Interaction module of COMSOL Multiphysics to simulate the generation and coupling of photoacoustic waves as well as the displacement of the piezoelectric solid. The configuration of the QTF and the fiber is shown in Fig. 1. The three-dimensional position of the fiber is varied by the vertical offset along the z axis, and the horizontal offset along the y axis. In the three-dimensional model, only half of the tuning fork needs to be considered due to structural symmetry as indicated in Fig. 2. The dimensions of the QTF are similar to those in previous works [16,19], each prong being 3.8 mm × 0.6 mm × 0.34 mm with the gap between the prongs being 0.3 mm and the base length being 2.33 mm. The external cylinder in Fig. 2 represents the gas domain, in which an outer shell is designed as a perfectly matched layer (PML) to prevent boundary reflections; this domain is kept small in size to preserve memory space. The two overlapping (blue) cylinders in Fig. 2 represent the acoustic source corresponding to the light field generated at the tip of the fiber. For the inner cylinder, which has a radius of 40 μm, a self-defined extremely refined mesh is needed for the analysis. The radius of the outer cylinder is set to 0.13 mm, slightly smaller than half of the tuning fork gap. The height of the acoustic source is chosen to be 2 mm to ensure that most of the energy of the light beam emitted from the fiber is included in the model. As only a qualitative analysis is needed in this simulation, the proportionality coefficient between the self-defined acoustic source and the power distribution, I, can be chosen arbitrarily. All dimensions and parameters in the respective models of a common fiber and an axicon fiber are kept the same for the convenience of comparison.

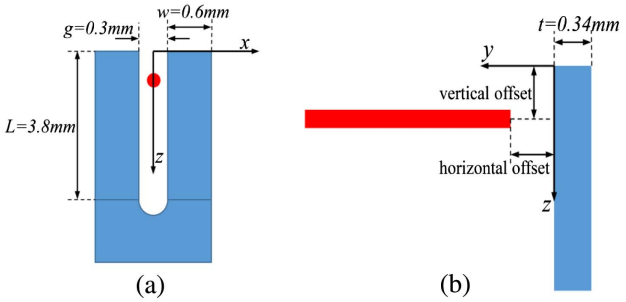

Fig. 1. Schematics of the quartz tuning fork (QTF) and fiber configuration; (a) transverse and (b) flank side of the QTF. L, w, and t represent the length, width, and thickness of the QTF prong and g the QTF gap.

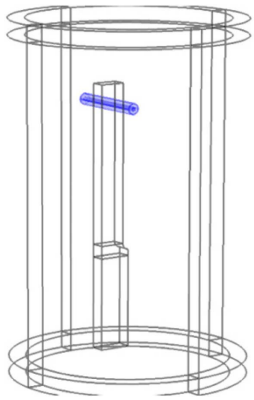

Fig. 2. Schematic diagram of the geometry of the numerical model for the fiber-based quartz-enhanced photoacoustic spectroscopy system. The external cylinder represents the gas domain, the horizontal (blue) cylinder the acoustic source, and the rectangular shape (half of) the tuning fork.

3. EXPERIMENTAL SETUP

The experimental setup is depicted in Fig. 3. A tunable laser (Agilent, Inc., 81940A) serves as the light source, and an optical amplifier (Amonics, Ltd., AEDFA-33-B) is used to amplify the light power up to 40 mW. In the experiments, the wavelength and modulation frequency of the laser are set at 1530.368 nm in an absorption line of C_2H_2 and 32.75 kHz in the measured resonant frequency of QTF in pure nitrogen, respectively. The frequency of QTF at its first flexion resonance mode has no change when C_2H_2 is added. The Q value of QTF, defined

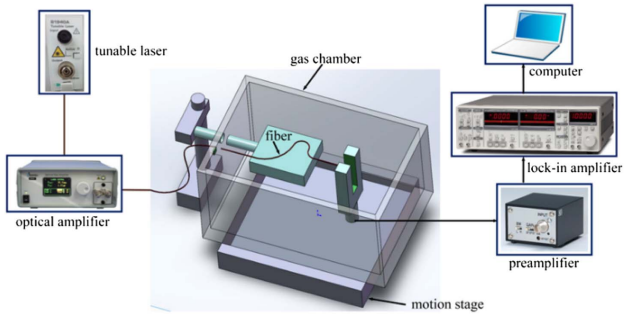

Fig. 3. Schematic diagram of the fiber-based QEPAS system.

as FWHM divided by resonant frequency, is about 9600. The QTF is mounted inside a self-made compact cuboid gas chamber, which in turn is fixed on a three-dimensional compact linear stage (Newport, Co., VP-25XA). The gas chamber size is approximately 15 cm × 10 cm × 8 cm. The chamber contains a gas inlet and a gas outlet, a fiber connector, and an electric signal interface. It has a hole on the left side of the chamber sealed with a hollow balloon on a steady optical post, the purpose of which is to allow the displacement of post in the hole while maintaining good leakproofness. In the experiments the fiber fixed on the platform by a self-made V groove and tape is connected to the post and kept motionless while the position of the QTF is controlled by the motion stage to obtain optimal alignment. The output current signal from the QTF is amplified by a preamplifier (Hamamatsu Photonics, Ltd., C7319) with a current-to-voltage conversion factor of 10 V/μA, and is then detected by a lock-in amplifier (Stanford Research System, Inc., Model SR 830) and recorded by a LABVIEW (National Instrument, Inc., Labview 2011) based program. The time constant of the lock-in amplifier is set to 100 ms with a 6 dB/Oct slope filter.

4. RESULTS

A. Numerical Results

The resonant frequency of the QTF is calculated by the finite element model to be 36.13 kHz and found to be in accordance with the analytical result described in Ref. [18]. To produce the strongest photoacoustic signal, we use simulations to find the optimal light beam offset from the top of the QTF. The displacement of the QTF is calculated with the acoustic source at different positions along the perpendicular middle axis (z axis as shown in Fig. 1(a)) of the QTF. The horizontal position of the acoustic source cylinder along the y axis as shown in Fig. 1(b) is fixed at 0.2 mm. Two kinds of acoustic sources are used, a Gaussian beam from a common single-mode fiber with a flat end and a Bessel beam from an axicon fiber, respectively. Simulations using line sources [17] are also used for comparisons. In each case, all the displacements of the QTF are normalized to the maximum displacement. The results are depicted in Fig. 4. The optimal vertical offsets along the z axis for the acoustic sources are all about 0.6 mm, which agrees well with previous theoretical [20,21] and experimental results [4]. Thus the correctness of our simulation model has been verified. It is indicated from Fig. 4 that using the light source with a simple line model instead of a complete beam profile model is also valid, especially near the best vertical position. However, in the vertical positions away from the optimal point, the effect of beam profiles becomes more and more apparent.

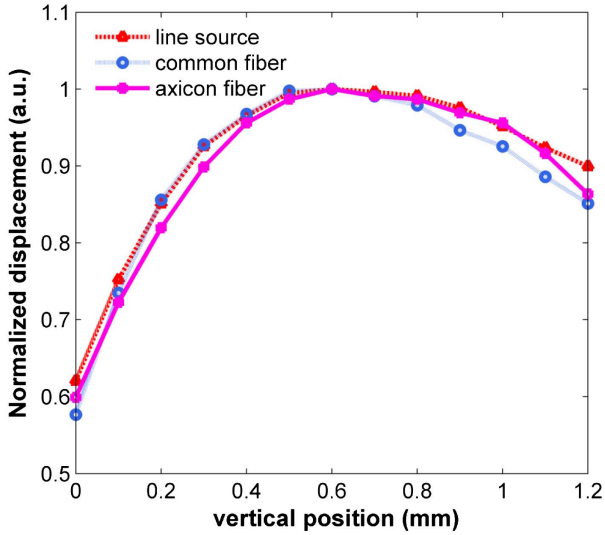

Fig. 4. Normalized simulated displacements of the QTF as a function of vertical offsets (z in Fig. 1(a)) for three different light sources: a simplified line source, a Gaussian light source from common a single-mode fiber, and a Bessel light source from an axicon fiber.

To study the optimal three-dimensional position of the fibers, the vertical offsets of the acoustic sources are fixed at 0.6 mm. The displacements of tuning fork prongs are then simulated at varying horizontal distances between the QTF and the fiber along the y axis. As shown in Fig. 5, the optimal horizontal offset of the single-mode fiber is 0.6 mm, at which

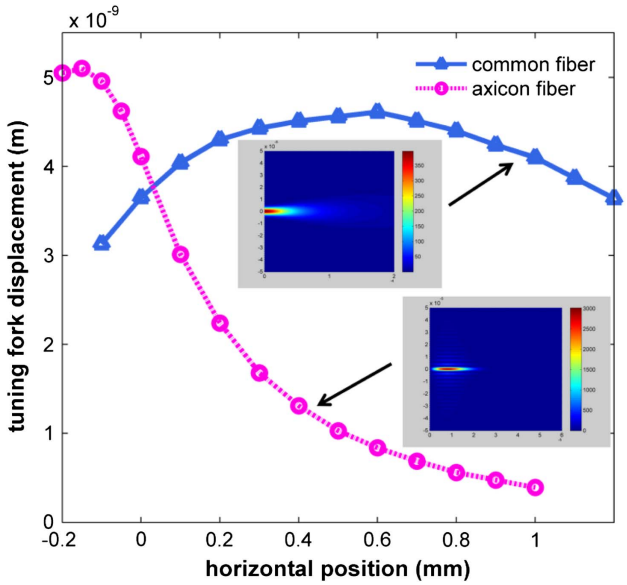

Fig. 5. Simulated tuning fork displacements on different horizontal positions of two kinds of fibers: common single fiber and axicon fiber. Insets show the output beam profile on the YZ view of common fiber and axicon fiber, and color bars represent the beam intensity.

distance approximately 60% of the QTF gap cross section is covered by the Gaussian beam. The optimal offset of the axicon fiber with the focus beam is −0.15 mm, indicating that the axicon fiber should be placed between QTF prongs to place the focused light in the center of the QTF. The tuning fork displacement of axicon fiber decreases dramatically with distance from the center because most of the output energy of the beam is focused in a spot with a small focal depth. However, the beam energy from a single-mode fiber changes slowly, so it has a smooth curve. Beam profiles from the YZ view of two kinds of fiber, which are calculated from Eqs. (2) and (3), could be seen from the insets of Fig. 5. The maximal displacement of the QTF, i.e., the strongest photoacoustic signal, generated by the axicon fiber is about 1.1 times larger than the strongest signal generated by the common single-mode fiber, which seems to suggest that a focused beam is a somewhat better photoacoustic excitation source. The difference is, however, not significant, which most likely can be attributed to the fact that the output light power from the two types of fibers is essentially the same albeit with different beam distributions.

B. Experimental Results

To investigate the sensitivity of the fiber-based compact QEPAS system we measure the photoacoustic signals generated by the two different fibers at different C_2H_2 concentrations. In each case, the fiber is fixed on the platform inside the gas chamber and C_2H_2 mixed with N_2 is infused into the chamber. Based on the optimal position of the QTF as calculated in the simulations in the previous section, the location of the QTF is adjusted together with the gas chamber by controlling the three-dimensional motion stage to obtain the strongest photoacoustic signal. The output signals of different gas concentrations are then recorded. The results for the single-mode fiber and the axicon fiber are shown in Figs. 6 and 7, respectively. In both cases the signals display a linear relationship with the gas concentrations. The main experimental error is caused by the mass flow meter used to control the acetylene concentration in the gas mixture. The standard derivations of noises are almost the same at different concentrations as shown in Figs. 6 and 7. One thing to be mentioned is that diffraction from the axicon fiber can cause a large noise when the fiber is put farther away from the tuning fork than about 1 mm. In the normal case, the noise is mainly due to thermal noise of the QTF and noise in the electrical detection, and it is estimated to be 1.1 μV from the data in Fig. 7, which yields a signal-to-noise ratio (SNR) of about 95 at 2.44% acetylene. We can thus derive the detection limit for the axicon fiber to be 259 ppm, which is comparable to that reported for TOFs [13]. We find the detected signal values for the common fiber and the axicon fiber to be comparable, with the signal of the axicon fiber being only 1.05 times larger than that of common single-mode fiber. Considering that the best position of axicon fiber requires very precise adjustment and that the difference in detected signal values is small we can conclude that for practical applications the common single-mode fiber is preferable.

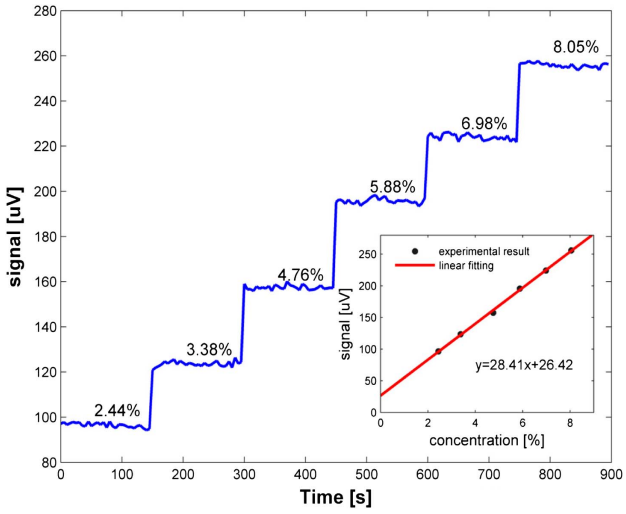

Fig. 6. Photoacoustic signals induced by the common single-mode fiber repetitively recorded with different acetylene concentrations. The inset shows the averaged signal as a function of acetylene concentration.

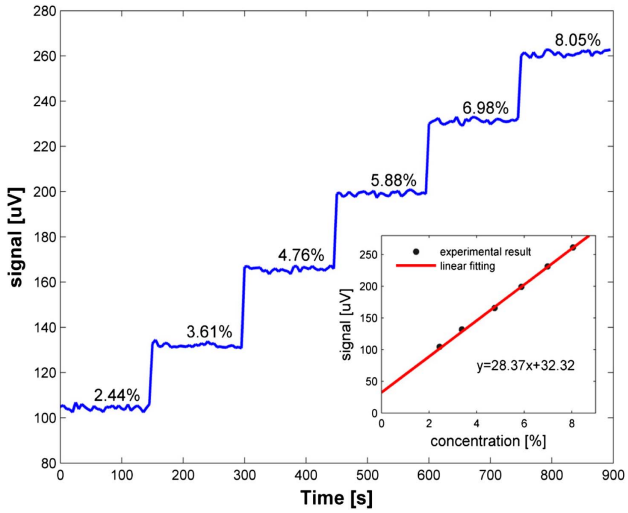

Fig. 7. Equivalent results to those in Fig. 6 for the axicon fiber.

We note that the experimental results also agree well with the results of our numerical simulations.

5. CONCLUSION

In this paper, we have reported the development of a finite element model that simulates the deformation of a QTF photoacoustic sensor caused by light-induced sound waves. To our knowledge, this is the first time that actual light beam profiles (as opposed to a simplified line source) are used in simulations of such a photoacoustic sensor. Based on this numerical model, we calculated the optimal spatial position of the light beams in three dimensions for a common single-mode fiber with a flat end as well as for an axicon fiber. These results provide meaningful input for experiments as well as for future applications to obtain maximized photoacoustic signals.

We have furthermore reported on the development of a novel compact fiber-based photoacoustic sensor that does not require additional collimators or focus lenses. Unlike

similar systems based on tapered fibers with diameters of the order of 1 μm requiring sophisticated fabrication methods as well as careful maintenance to avoid breaking, our system uses a common single-mode fiber but is even so able to detect gas concentrations with almost the same sensitivity while being more stable and having an easier arrangement configuration. For C_2H_2, the detection limit by our system is about 259 ppm, which suffices in practical cases.

An axicon fiber has also been tested in the system to verify whether a focused beam is more effective for photoacoustic excitation. We find our experimental results to be in good agreement with those from our simulations. The two kinds of fibers generate almost the same photoacoustic signals. Since the optimal location of the axicon fiber needs to be quite precisely adjusted, the common single-mode fiber offers the better choice for the development of a miniature, compact, stable, and portable fiber-based QEPAS sensor for practical application in future work.

China Postdoctoral Science Foundation (2014M551729); Fundamental Research Funds for the Central Universities; National Natural Science Foundation of China (NSFC) (61401392); Science and Technology Department of Zhejiang Province (2010R50007).

The authors thank Kaikai Guo, Hao Lu, Senlin Zhang, and Yongquan Chen, all at Zhejiang University, for their help in experimental preparation.

†These authors contributed equally to this study.

REFERENCES

1. A. Elia, P. M. Lugara, C. Di Franco, and V. Spagnolo, "Photoacoustic techniques for trace gas sensing based on semiconductor laser sources," Sensors **9**, 9616–9628 (2009).
2. S. Schilt, L. Thevenaz, M. Nikles, L. Emmenegger, and C. Huglin, "Ammonia monitoring at trace level using photoacoustic spectroscopy in industrial and environmental applications," Spectrochim. Acta A **60**, 3259–3268 (2004).
3. J. P. Lima, H. Vargas, A. Miklos, M. Angelmahr, and P. Hess, "Photoacoustic detection of NO_2 and N_2O using quantum cascade lasers," Appl. Phys. B **85**, 279–284 (2006).
4. J. S. Li, X. M. Gao, W. Z. Li, Z. S. Cao, L. H. Deng, W. X. Zhao, M. Q. Huang, and W. J. Zhang, "Near-infrared diode laser wavelength modulation-based photoacoustic spectrometer," Spectrochim. Acta A **64**, 338–342 (2006).
5. A. Schmohl, A. Miklós, and P. Hess, "Detection of ammonia by photoacoustic spectroscopy with semiconductor lasers," Appl. Opt. **41**, 1815–1823 (2002).
6. A. A. Kosterev, Y. A. Bakhirkin, R. F. Curl, and F. K. Tittel, "Quartz-enhanced photoacoustic spectroscopy," Opt. Lett. **27**, 1902–1904 (2002).
7. L. Dong, J. Wright, B. Peters, B. A. Ferguson, F. K. Tittel, and S. McWhorter, "Compact QEPAS sensor for trace methane and ammonia detection in impure hydrogen," Appl. Phys. B **107**, 459–467 (2012).
8. A. A. Kosterev, F. K. Tittel, D. V. Serebryakov, A. L. Malinovsky, and I. V. Morozov, "Applications of quartz tuning forks in spectroscopic gas sensing," Rev. Sci. Instrum. **76**, 043105 (2005).
9. S. Böttger, M. Köhring, U. Willer, and W. Schade, "Off-beam quartz-enhanced photoacoustic spectroscopy with LEDs," Appl. Phys. B **113**, 227–232 (2013).
10. J. M. Friedt and E. Carry, "Introduction to the quartz tuning fork," Am. J. Phys. **75**, 415–422 (2007).
11. K. Liu, X. Y. Guo, H. M. Yi, W. D. Chen, W. J. Zhang, and X. M. Gao, "Off-beam quartz-enhanced photoacoustic spectroscopy," Opt. Lett. **34**, 1594–1596 (2009).
12. V. Spagnolo, P. Patimisco, S. Borri, G. Scamarcio, B. E. Bernacki, and J. Kriesel, "Part-per-trillion level SF_6 detection using a quartz enhanced photoacoustic spectroscopy-based sensor with single-mode fiber-coupled quantum cascade laser excitation," Opt. Lett. **37**, 4461–4463 (2012).
13. L. Dong, A. A. Kosterev, D. Thomazy, and F. K. Tittel, "QEPAS spectrophones: design, optimization, and performance," Appl. Phys. B **100**, 627–635 (2010).
14. K. Liu, J. Li, L. Wang, T. Tan, W. Zhang, X. Gao, W. Chen, and F. K. Tittel, "Trace gas sensor based on quartz tuning fork enhanced laser photoacoustic spectroscopy," Appl. Phys. B **94**, 527–533 (2009).
15. M. D. Wojcik, M. C. Phillips, B. D. Cannon, and M. S. Taubman, "Gas-phase photoacoustic sensor at 8.41 μm using quartz tuning forks and amplitude-modulated quantum cascade lasers," Appl. Phys. B **85**, 307–313 (2006).
16. M. Jahjah, A. Vicet, and Y. Rouillard, "A QEPAS based methane sensor with a 2.35 μm antimonide laser," Appl. Phys. B **106**, 483–489 (2012).
17. Y. C. Cao, W. Jin, L. H. Ho, and Z. B. Liu, "Evanescent-wave photoacoustic spectroscopy with optical micro/nano fibers," Opt. Lett. **37**, 214–216 (2012).
18. L. M. Tong, J. Y. Lou, Z. Z. Ye, G. T. Svacha, and E. Mazur, "Self-modulated taper drawing of silica nanowires," Nanotechnology **16**, 1445–1448 (2005).
19. T. Grosjean, S. S. Saleh, M. A. Suarez, I. A. Ibrahim, V. Piquerey, D. Charraut, and P. Sandoz, "Fiber microaxicons fabricated by a polishing technique for the generation of Bessel-like beams," Appl. Opt. **46**, 8061–8067 (2007).
20. N. Petra, J. Zweck, A. A. Kosterev, S. E. Minkoff, and D. Thomazy, "Theoretical analysis of a quartz-enhanced photoacoustic spectroscopy sensor," Appl. Phys. B **94**, 673–680 (2009).
21. Y. Cao, W. Jin, and H. L. Ho, "Optimization of spectrophone performance for quartz-enhanced photoacoustic spectroscopy," Sens. Actuators B **174**, 24–30 (2012).
22. S. L. Firebaugh, F. Roignant, and E. A. Terray, "Enhancing sensitivity in tuning fork photoacoustic spectroscopy systems," in *IEEE Sensors Applications Symposium (SAS)* (IEEE, 2010), pp. 30–35.
23. N. Petra, J. Zweck, S. E. Minkoff, A. A. Kosterev, and J. H. Doty, "Modeling and design optimization of a resonant optothermoacoustic trace gas sensor," SIAM J. Appl. Math. **71**, 309–332 (2011).
24. H. Yi, K. Liu, S. Sun, W. Zhang, and X. Gao, "Theoretical analysis of off beam quartz-enhanced photoacoustic spectroscopy sensor," Opt. Commun. **285**, 5306–5312 (2012).
25. B. E. A. Saleh and M. C. Teichl, *Fundamentals of Photonics* (Wiley, 1991).
26. O. Brzobohaty, T. Cizmar, and P. Zemanek, "High quality quasi-Bessel beam generated by round-tip axicon," Opt. Express **16**, 12688–12700 (2008).